

# Quasiparticle band structure of bulk hexagonal boron nitride and related systems

X. Blase, Angel Rubio, Steven G. Louie, and Marvin L. Cohen

*Department of Physics, University of California at Berkeley, Berkeley, California 94720  
and Materials Sciences Division, Lawrence Berkeley Laboratory, Berkeley, California 94720*

(Received 19 September 1994)

The quasiparticle band structure of bulk hexagonal boron nitride is studied within the *GW* approximation for the self-energy operator. The influence of the interlayer distance on the band structure is investigated both within the local density approximation and the quasiparticle approach, and the importance of an interlayer state in determining the gap is demonstrated. Also, the quasiparticle band structure for an isolated sheet of boron nitride is calculated. We show that the equivalent of the interlayer state in the case of the isolated boron nitride sheet plays the same role as in the bulk case in determining the band gap.

## I. INTRODUCTION

Recently, using an analogy between carbon- and BN-based materials, the existence of BN nanotubes has been suggested.<sup>1,2</sup> Because these nanotubes can be viewed as being generated by rolling a sheet of hexagonal BN onto itself, this simple structure has been the object of renewed interest.<sup>2,3</sup> Further, it has been shown<sup>2</sup> that, in the case of multiwall or small single-wall nanotubes, the effect of intra- or interwall interactions on the electronic levels could be reproduced in a band-folding analysis by allowing the isolated BN sheet to interact more or less strongly with neighboring BN layers. In addition, the intrinsic properties of bulk BN strongly motivate this study, since cubic BN is an extremely hard material<sup>4</sup> and displays the largest heteropolar gap of all III-V compounds. In this work, both bulk hexagonal BN and the isolated BN sheet are investigated. To our knowledge, this is the first quasiparticle calculation for bulk hexagonal boron nitride.<sup>5</sup> We also have examined intermediate structures composed of a periodic repetition of BN layers with an interlayer distance varying from  $d=5.5$  Å to  $d=13.5$  Å and analyzed the effect of the interlayer interaction on the band structures. We will use the notation BN( $d$ ) for these compounds.

Because the density functional theory is a ground-state formalism, standard local density approximation (LDA) band structure calculations do not yield the true quasiparticle energy levels. In particular, it is well known that the LDA underestimates the band gap of most semiconductors. In this work, we show that the LDA not only underestimates the gap of the structures under study, but also yields an incorrect ordering of the conduction bands in the case of the isolated BN sheet. In fact, for this system, the self-energy correction is strongly band dependent and  $\mathbf{k}$  dependent and therefore plays a more drastic role than one would expect from the simple “scissor” approach sometimes used to describe the results of self-energy corrections. The quasiparticle calculations are carried out using the Hybertsen-Louie method<sup>6</sup>

which is based on Hedin’s *GW* approximation<sup>7</sup> for the electron self-energy operator. This approach has been shown to yield for semiconductors bulk,<sup>6,8,9</sup> surface,<sup>10,11</sup> interface,<sup>12</sup> and superlattice<sup>13</sup> quasiparticle energies accurate to within 0.1 eV when compared to experiment. Recently, the method has also been successfully applied to complex molecular solids such as solid C<sub>60</sub>.<sup>14</sup>

The paper is organized as follows. In Sec. II, the theoretical methods and the technical details are discussed for the LDA and quasiparticle calculations. In Sec. III, the LDA band structures are given and the wave functions of the states controlling the band gaps are plotted. In particular, it is shown that an interlayer state forms the bottom of the conduction band in most structures. In the case of an isolated sheet, the interlayer state transforms into a state with a large extension into the vacuum, away from the plane of atoms. In Sec. IV, the quasiparticle band structures are given and the differences between the quasiparticle and the LDA results are discussed. Discrepancies with a previous quasiparticle band structure calculation performed on an isolated BN sheet<sup>3</sup> are analyzed. In Sec. V, a summary and conclusions are given.

## II. THEORETICAL METHODS

### A. LDA *ab initio* pseudopotential calculations

We carry out *ab initio* pseudopotential LDA calculations, using a plane-wave expansion for the pseudopotentials and wave functions. The energy cutoff for the electronic wave functions is set at  $E_{\text{cut}}=36$  Ry. Boron and nitrogen pseudopotentials are generated following the Troullier and Martins pseudopotential generation scheme.<sup>15</sup> The Ceperley-Alder exchange and correlation potential<sup>16</sup> is used. The BN bond length is set to the experimental distance of 1.45 Å. The distance between two layers is chosen to be 3.34 Å for hexagonal BN. For this structure, *AB* stacking with each B atom on top of

a N atom is imposed in each unit cell. A  $4 \times 4 \times 2$  grid in the Monkhorst and Pack scheme<sup>17</sup> is used to generate 20 points in the irreducible Brillouin zone (BZ). The conventional notation for the hexagonal BZ is reproduced in Fig. 1. Among these 20 irreducible  $\mathbf{k}$  points, ten are located in the  $\Gamma MK$  area and ten in the  $ALH$  area.

For BN( $d$ ) structures, we choose an AA stacking with B atoms (respectively N atoms) on top of each other. This permits us to reduce the size of the unit cell by a factor of 2 as compared to the stacking in bulk hexagonal BN, and makes no difference in the limit of the isolated sheet. In addition, both the isolated sheet and the intermediate BN( $d$ ) structures have the  $D_{6h}$  symmetry, while bulk hexagonal BN transforms according to the symmetries of the smaller  $C_{6h}$  group. The interlayer distance is varied between  $d = 5.5 \text{ \AA}$  and  $d = 13.5 \text{ \AA}$  until stabilization of the electronic energy levels is achieved. We then obtain the band structure of the isolated BN sheet within this supercell approach.

### B. First-principles quasiparticle approach to electron excitation energies

In the self-energy approach used to compute the quasiparticle energies,<sup>6,7</sup> the quasiparticle equation of motion is written

$$[\hat{T} + V_{\text{ext}}(\mathbf{r}) + V_H(\mathbf{r})]\Psi^{\text{qp}}(\mathbf{r}) + \int d^3\mathbf{r}' \Sigma(\mathbf{r}, \mathbf{r}'; E^{\text{qp}})\Psi^{\text{qp}}(\mathbf{r}') = E^{\text{qp}}\Psi^{\text{qp}}(\mathbf{r}), \quad (1)$$

where  $\hat{T}$  is the kinetic energy operator,  $V_{\text{ext}}$  the external potential, and  $V_H$  a mean-field electron-electron interaction potential (the Hartree potential in this case.) The self-energy operator  $\Sigma$ , which includes the effects of exchange and correlation, is nonlocal, energy dependent, and non-Hermitian in general.

Following Hedin's work,<sup>7</sup>  $\Sigma$  is taken to be the first-order term in an expansion in successive powers of the screened Coulomb interaction  $W$ :

$$\Sigma(\mathbf{r}, \mathbf{r}'; E^{\text{qp}}) = i \int \frac{dE'}{2\pi} e^{-i\delta E'} G(\mathbf{r}, \mathbf{r}'; E - E') W(\mathbf{r}, \mathbf{r}'; E'), \quad (2)$$

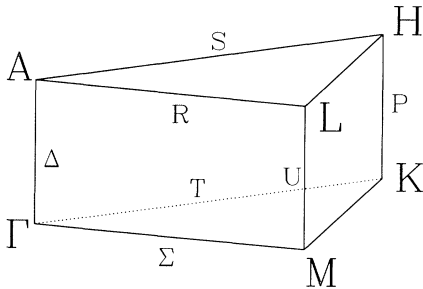


FIG. 1. High-symmetry points and directions are labeled for the irreducible part of the hexagonal Brillouin zone.

where  $G$  is the dressed one-particle Green's function. This is the so-called  $GW$  approximation. Our approach<sup>6</sup> is to make the best possible approximation for  $G$  and  $W$ . As shown in previous  $GW$  calculations in semiconductors, the LDA wave functions accurately describe the quasiparticle wave functions in semiconductors so that we may approximate

$$G(E) = \sum_{n\mathbf{k}} \frac{|n\mathbf{k}\rangle\langle n\mathbf{k}|}{E - E_{n\mathbf{k}} - i\eta}, \quad (3)$$

with  $|n\mathbf{k}\rangle$  being the LDA eigenfunctions and  $E_{n\mathbf{k}}$  the self-consistent quasiparticle energies ( $\eta$  is a negative infinitesimal for energies above the Fermi energy and a positive infinitesimal below).

The screened Coulomb interaction  $W = V \times \epsilon^{-1}$  is calculated in Fourier space using the Hybertsen-Louie scheme.<sup>6,18</sup>  $V$  is the bare Coulomb potential and  $\epsilon^{-1}$  the inverse dynamical dielectric matrix. In calculating  $\epsilon^{-1}$ , the static polarizability  $P$  is evaluated in the Adler-Wiser formulation<sup>19,20</sup> within the random phase approximation (RPA). Local field effects are taken into account so that the polarizability matrix is nondiagonal in reciprocal space. After inversion of the static dielectric matrix  $\epsilon(\mathbf{q}, \omega = 0)$ , we extend  $\epsilon^{-1}$  to finite frequencies using a generalized plasmon pole model<sup>18</sup> which yields a different pole at  $\tilde{\omega}_{\mathbf{G}, \mathbf{G}'}(\mathbf{q})$  for each element  $\epsilon_{\mathbf{G}, \mathbf{G}'}^{-1}(\mathbf{q}; \omega)$  of the inverse dielectric matrix. The strength and position of each pole are uniquely determined by imposing that  $\epsilon_{\mathbf{G}, \mathbf{G}'}^{-1}(\mathbf{q}; \omega)$  satisfies both the Kramers-Kronig relations and a generalized  $f$ -sum rule.<sup>6</sup>

The quasiparticle excitation energies are then calculated using the expression

$$E_{n\mathbf{k}}^{\text{qp}} = E_{n\mathbf{k}}^{\text{LDA}} + \langle n\mathbf{k} | \Sigma(E_{n\mathbf{k}}^{\text{qp}}) - V^{\text{LDA}} | n\mathbf{k} \rangle. \quad (4)$$

Since Eq. (4) is a self-consistent equation, we start by calculating the self-energy operator at the LDA eigenvalues and iterate by using the updated eigenvalues until convergence. Usually, one or two iterations are enough to converge the eigenvalues to within 0.1 eV. The validity of Eq. (4) is based on the fact that the LDA and quasiparticle wave functions are, in general, in excellent agreement.<sup>6</sup> Thus one needs only to calculate the diagonal elements of the difference Hamiltonian,  $\Sigma(E_{n\mathbf{k}}^{\text{qp}}) - V^{\text{LDA}}$ .

The dielectric matrix is truncated at  $|\mathbf{q} + \mathbf{G}| = 3$  a.u. This is enough to describe the local field effects in the present cases. The  $\mathbf{k}$ -point sampling used for the BZ summations involved in the calculation of both the dielectric matrix and the self-energy matrix elements is the same as those used in the LDA calculations. We include 40 bands per atom in the unit cell to perform the summation over the conduction bands for the calculation of the RPA independent-particle polarizability. The same number of bands is used to calculate the Green's function. Finally, a cutoff of  $|\mathbf{q} + \mathbf{G}| = 4$  a.u. is used to converge the bare-exchange contribution to the self-energy correction. Coulomb-hole and screened-exchange terms converge faster, and we set  $|\mathbf{q} + \mathbf{G}| \leq 3$  a.u. for these calculations. This gives quasiparticle energies converged to within 0.1 eV.

### III. RESULTS

#### A. LDA calculations

In Fig. 2, the LDA band structure for bulk hexagonal boron-nitride is plotted along high-symmetry directions of the BZ. The energy levels at high-symmetry points are reported in Table I. Because of layer-layer interactions, the dispersion along the  $c$  axis is non-negligible as can be seen from the band structure along the  $\Gamma A$ ,  $ML$ , and  $KH$  directions. Within the LDA, we find that bulk hexagonal BN is a large-gap semiconductor, with an indirect gap of 3.9 eV between the top of the valence band near  $K$  and the bottom of the conduction band at  $M$ . The top of

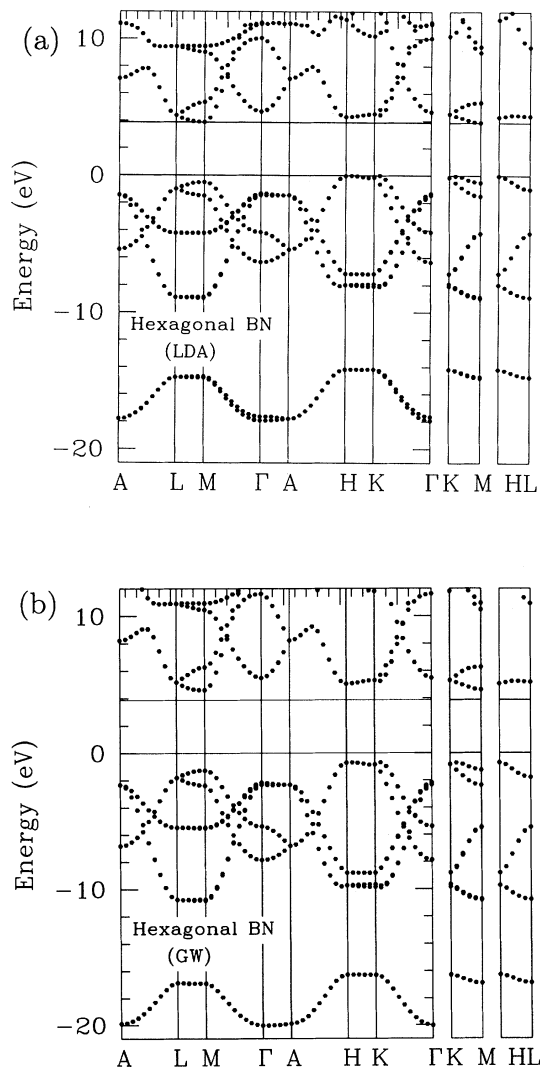


FIG. 2. (a) LDA band structure and (b)  $GW$  band structure for bulk hexagonal boron nitride plotted along high-symmetry directions of the BZ. The energies are in eV. The top of the valence band within the LDA is taken to be the zero of energies. The edges of the LDA gap are indicated by horizontal lines as a guide to the eyes.

the valence band, located near  $K$  along  $K\Gamma$  (we will use the notation  $T_1$  for this point), is very close in energy to the highest occupied molecular orbital (HOMO) state at  $H$  (within room temperature in our calculations). The direct gap at  $\Gamma$  is found to be 5.95 eV. Both the indirect band gap and the direct gap at  $\Gamma$  are smaller than in cubic<sup>21,22</sup> and wurtzite<sup>22</sup> BN. The direct band gap at  $\Gamma$  is the most structure sensitive. It changes by 2.5–3 eV between the cubic or wurtzite and hexagonal structures (as discussed below, this is due to the “interlayer” nature of the conduction band minimum in the case of the hexagonal structure). This should help to identify the structurality of tubular BN in its recently predicted novel forms.<sup>23</sup> In Fig. 3(a), 3(b), and 3(c), electron densities are given for the bottom of the conduction band at  $M$  and the highest occupied state at  $K$  and  $H$ , respectively. For the lowest unoccupied molecular orbital (LUMO) state at  $M$ , the charge density is localized on the boron atoms while for the HOMO state at  $K$  and  $H$ , the charge density is localized on the nitrogen atoms. All of these states display a  $\pi$ - or  $\pi^*$ -like character. We note the difference of charge localization for the HOMO states at  $K$  and  $H$ . In addition, a phonon-assisted optical transition from  $H$  to  $M$  would require phonons propagating along the  $c$  axis. We expect these two features to help in the identification of the states involved in either  $p$ -type doping or optical experiments.

We study also the lowest unoccupied state at  $\Gamma$ . The corresponding charge density is represented in Fig. 3(d). This state has most of its charge concentrated in the interlayer region. The  $xy$ -average charge density plotted along the  $c$  axis shows a strong maximum at the midpoint between the two neighboring BN layers. This state is the analog of the interlayer state in graphite.<sup>26</sup> The remaining charge on the BN planes is located mostly on the nitrogen atoms. This is in contrast to graphite where the on-plane charge for the interlayer state is equally distributed on each carbon atom. The difference in ionicity between B and N explains this feature for hexagonal BN.

As intermediate structures between bulk hexagonal BN

TABLE I. Bulk hexagonal BN eigenvalues at high-symmetry points. The energies are in eV. The top of the valence band is taken to be the zero of energies for both LDA and  $GW$  results.

| k point       | LDA    | $GW$   |
|---------------|--------|--------|
| $\Gamma_{1v}$ | -17.94 | -19.87 |
| $\Gamma_{3v}$ | -17.65 | -19.57 |
| $\Gamma_{3v}$ | -6.33  | -7.33  |
| $\Gamma_{1v}$ | -4.12  | -4.80  |
| $\Gamma_{5v}$ | -1.45  | -1.69  |
| $\Gamma_{6v}$ | -1.32  | -1.57  |
| $\Gamma_{1c}$ | 4.63   | 5.96   |
| $\Gamma_{3c}$ | 10.06  | 12.61  |
| $K_{3v}$      | -14.14 | -15.91 |
| $K_{1v}$      | -8.05  | -9.01  |
| $K_{2v}$      | -7.89  | -8.82  |
| $K_{3v}$      | -7.17  | -8.45  |
| $K_{3v}$      | -0.14  | -0.14  |
| $K_{3c}$      | 4.50   | 6.19   |

and an isolated sheet, we study the  $\text{BN}(d)$  “gedanken” compounds. We vary the interlayer distance  $d$  from 5.5 Å to 13.5 Å. Stabilization of the band structure is observed for  $d$  larger than 11.5 Å. This is established by comparing with the band structure of the system with  $d = 13.5$  Å. With the interlayer distance increasing from  $d = 5.5$  Å to larger values, the energy of the valence states and lowest unoccupied states hardly changes, except for the lowest unoccupied state at  $\Gamma$  which moves up in energy. This is not surprising since this state is the analog of the interlayer state in bulk hexagonal BN and has a very large extension into the interlayer region. We show in Fig. 4 the evolution of the charge density for this state for  $d = 5.5, 9.5,$  and  $13.5$  Å. As one can see, the corresponding wave functions from neighboring planes strongly overlap for  $d = 5.5$  Å and  $d = 9.5$  Å. Only for  $d = 13.5$  Å does this overlap begin to be negligible and we get noninteracting BN layers. In the case of  $d = 13.5$  Å, we also plot the average potential along the  $c$  axis. This potential is very flat in the middle of the interlayer region, ensuring that indeed BN layers are not interacting. We list in Table II the energy of the band gap edge states at  $\Gamma, K,$  and  $M$ . The eigenvalues stabilize for

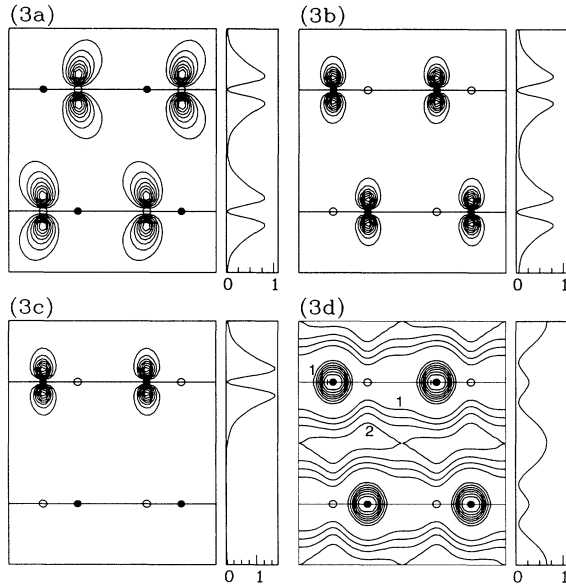


FIG. 3. Contour plots in a plane perpendicular to the BN layers of the charge density of selected states for bulk hexagonal BN. BN layers are indicated by horizontal lines. N atoms are represented with filled circles and B atoms with empty circles. In addition, the charge density averaged over planes parallel to the BN layers is represented as a function of the distance perpendicular to the BN layers; this charge density is normalized to unity within one unit cell. (a), (b), (c), and (d) correspond, respectively, to the LUMO state at  $M$ , the HOMO state at  $K$ , the HOMO state at  $H$ , and the LUMO state at  $\Gamma$ . In (d), contours labeled 1 and 2 correspond to a charge density of, respectively,  $0.16 \times 10^{-4}$  and  $0.63 \times 10^{-4}$  electron/a.u.<sup>3</sup> The maximum charge density is  $1.26 \times 10^{-4}$  electron/a.u.<sup>3</sup> on the nitrogen atoms.

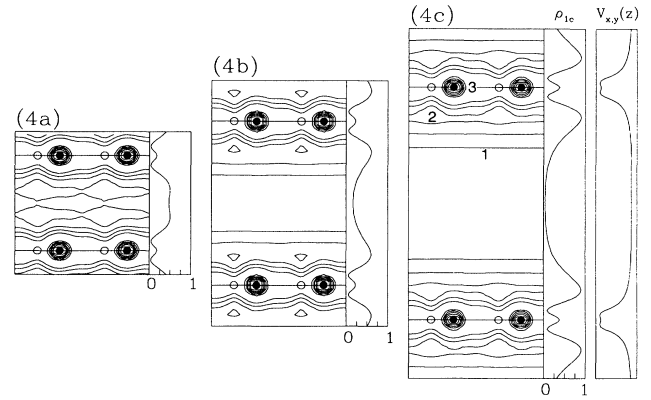


FIG. 4. Contour plot in a plane perpendicular to the BN layers of the charge density of the LUMO state at  $\Gamma$  for (a)  $\text{BN}(d=5.5)$ , (b)  $\text{BN}(d=9.5)$ , and (c)  $\text{BN}(d=13.5)$ . BN layers are indicated by horizontal lines. N atoms are represented with filled circles and B atoms with empty circles. In addition, the charge density averaged over planes parallel to the BN layers is represented as a function of the distance to the BN layers. This charge density is normalized to unity within one unit cell. In (c), contours labeled 1, 2, and 3 correspond to a charge density of, respectively,  $0.14 \times 10^{-4}$ ,  $0.43 \times 10^{-4}$ , and  $0.28 \times 10^{-4}$  electron/a.u.<sup>3</sup> The maximum charge density is  $0.85 \times 10^{-4}$  electron/a.u.<sup>3</sup> on the nitrogen atoms. The total potential averaged over planes parallel to the BN layers [ $V_{x,y}(z)$ ] is also represented.  $V_{x,y}(z)$  varies from  $-2.05$  Ry to the vacuum level (origin of energies).

$d \geq 11.5$  Å. We check that, for  $\text{BN}(d = 13.5)$  there is no dispersion along the  $\Gamma A$  direction, which confirms that, for such a layer-layer distance, two neighboring planes are not interacting. For  $d \leq 6.5$  Å, the bottom of the conduction band is at  $\Gamma$  within the LDA. For larger interlayer distances (and therefore for the isolated sheet), it is at  $K$ . For all structures, the top of the valence bands is at  $M$ . The LDA band structure for  $d = 13.5$  Å is represented in Fig. 5. Using our results for  $\text{BN}(d=13.5)$ , we conclude that, within the LDA, the isolated BN sheet is a 4.3 eV indirect gap semiconductor.

The lowest unoccupied level at  $\Gamma$  is a state which extends into the vacuum region with a maximum charge density at about 3.3 a.u. away from the plane of atoms. Such a state is difficult to understand in terms of B or N atomic orbitals. We note in Figs. 3(a), 3(b), and 3(c)

TABLE II. LDA HOMO and LUMO state energy at  $\Gamma, K,$  and  $M$  for various interlayer distances  $d$ . The energies are in eV. The top of the valence band  $K_{3v}$  is taken to be the zero of energies.

| State         | Interlayer distance (Å) |       |       |       |       |
|---------------|-------------------------|-------|-------|-------|-------|
|               | 5.5                     | 7.5   | 9.5   | 11.5  | 13.5  |
| $\Gamma_{6v}$ | -1.43                   | -1.50 | -1.57 | -1.57 | -1.57 |
| $\Gamma_{1c}$ | 3.97                    | 4.19  | 4.51  | 4.61  | 4.61  |
| $K_{3v}$      | 0.00                    | 0.00  | 0.00  | 0.00  | 0.00  |
| $K_{3c}$      | 4.41                    | 4.36  | 4.33  | 4.32  | 4.32  |
| $M_{3v}$      | -0.95                   | -0.97 | -0.99 | -0.99 | -0.99 |
| $M_{1c}$      | 4.57                    | 4.49  | 4.45  | 4.43  | 4.43  |

that the  $p_z$ -like orbitals associated with the BN sheet have a maximum charge density which is localized at most at 0.75 a.u. away from the atomic layer. Another important feature of the LUMO state at  $\Gamma$  is that its effective mass is calculated to be  $m^* = 0.95 \pm 0.05$  in units of the free-electron mass (the value varies slightly along the different planar directions). Therefore, this state displays a nearly-free-electron (NFE-) like charac-

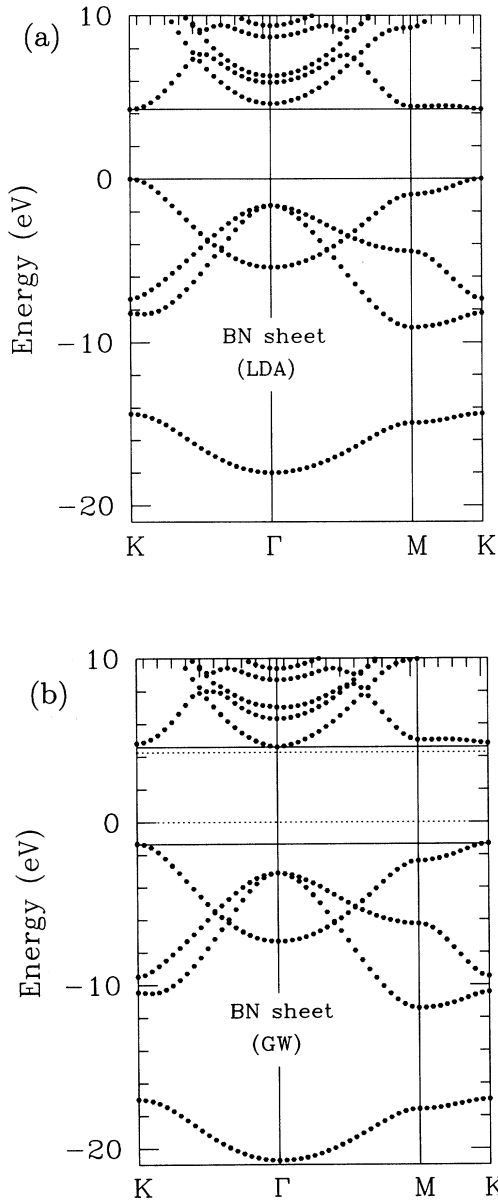


FIG. 5. (a) LDA band structure and (b) GW band structure for an isolated BN sheet plotted along high-symmetry directions of the BZ. The energies are in eV. The top of the valence band within the LDA is taken to be the zero of energies. In (a), the edges of the LDA gap are indicated by horizontal lines as a guide to the eyes. In (b), the edges of the GW gap are indicated by solid horizontal lines and the LDA gap by dashed horizontal lines as a guide to the eyes.

ter and an electron in this state would be mainly sensitive to the crystal potential averaged over the plane parallel to the BN layers. We write this potential  $V_{xy}(z)$ , where  $z$  is the distance of the electron from the BN layer to which it is bound.<sup>24</sup> Following this idea, we solve the one-dimensional Schrödinger equation for an electron in the  $V_{xy}(z)$  potential associated with an isolated BN sheet. In practice, we use the  $V_{xy}(z)$  potential we calculate for the BN( $d=13.5$ ) structure and set the vacuum level to the value of  $V_{xy}(z)$  at 6.5 Å away from a given BN layer. We plot this potential in Fig. 6 together with the charge density for the bound state ( $n=0,1,2$ ) solutions of this one-dimensional Schrödinger equation. The most important result is that the  $n=2$  level (located  $-0.55$  eV below the vacuum level) is very similar in shape to the charge density [represented in Fig. 4(c)] of the NFE state in BN( $d=13.5$ ). In particular, the  $n=2$  level charge density has a maximum at around 4.1 a.u. away from the BN layer. This is larger than the value of 3.3 a.u. we find for the NFE state but the qualitative agreement is satisfying considering the simplicity of the model. Thus our physical picture is that the NFE planar state is indeed the  $n=2$  loosely bound state due to the attractive planar average potential of a BN sheet but slightly modified by the discrete atomic potentials. The  $n=0$  and  $n=1$  states are so tightly bound to the BN sheet that they are strongly modified by the crystal potential and become indistinguishable from states obtained within a tight-binding description. We believe that such NFE plane states could be a very general feature of isolated crystalline sheets.<sup>25</sup>

## B. Self-energy calculations

We have performed self-energy calculations for bulk hexagonal BN, BN( $d=5.5$ ), BN( $d=7.5$ ), and

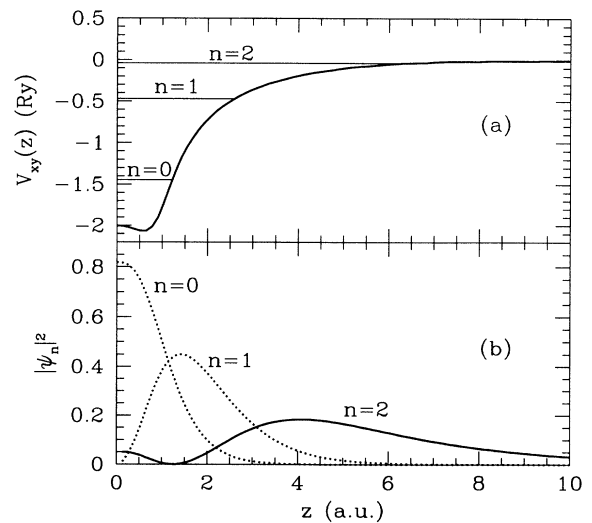


FIG. 6. (a)  $V_{x,y}(z)$  potential and (b) bound eigenstate charge densities are represented. The potential is in Ry and the distance in a.u. Positions of the eigenvalues with respect to the vacuum level are represented by horizontal lines in (a).

BN( $d=13.5$ ). As a first step, the static inverse dielectric matrix  $\epsilon_{GG'}^{-1}(\mathbf{q})$  is calculated within the random phase approximation. From this calculation, the macroscopic dielectric constant can be extracted using the relation  $\epsilon_M = \epsilon_{00}^{-1}(\mathbf{q} = \mathbf{0})$ . We find  $\epsilon_M=4.9$  for bulk hexagonal BN and  $\epsilon_M=3.3$  for both BN( $d=5.5$ ) and BN( $d=7.5$ ). This can be compared to the experimental value of  $\epsilon_M = 4.5$  for cubic BN,<sup>5</sup> and to the recently calculated value of 4.14 for both cubic and wurtzite BN.<sup>22</sup> Using the Philips and van Vechten empirical relation [see formula (6) of Ref. 5], one can see that the larger the average gap the smaller the macroscopic dielectric constant. Therefore the ordering of the dielectric constants for the cubic, wurtzite, and hexagonal bulk materials is consistent with the values for their respective gaps. However, owing to their different dimensionality, the plasmon energy for bulk BN structures and the isolated sheet may be significantly different and such an empirical relation cannot be straightforwardly used.

The quasiparticle band structure of bulk hexagonal BN is represented in Fig. 2(b). The main effect of the self-energy correction is to open the gap from 3.9 eV (LDA value) to 5.4 eV. Within the  $GW$  approximation, the calculated band gap is smaller for bulk hexagonal BN than for bulk cubic BN by 0.9 eV.<sup>5</sup> This is consistent with the closing of the gap going from diamond to graphite (in the case of BN, the ionicity gap prevents the occurrence of semimetallic behavior). Quasiparticle eigenvalues are reported in Table I together with the LDA energies for high-symmetry points. Because the self-energy is weakly  $\mathbf{k}$  dependent in this case, the  $GW$  band structure is very similar to the LDA band structure. In particular, the gap remains indirect between the top of the valence band at  $T_1$  near  $K$  and the bottom of the conduction band at  $M$ . We note that the self-energy correction for the highest occupied state at  $H$  and  $K$  are nearly identical so that the LDA energy difference between the top of the valence band and the HOMO state at  $K$  is not changed by the self-energy correction and both states remain very close in energy.

For BN( $d=5.5$ ), the self-energy correction  $\Delta E(E_{nk}^{\text{LDA}}) = E_{nk}^{\text{qp}} - E_{nk}^{\text{LDA}}$  is represented in Fig. 7. In contrast to bulk hexagonal BN, the self-energy correction  $\Delta E(E_{nk}^{\text{LDA}})$  is strongly  $\mathbf{k}$  dependent. In particular, the correction to the lowest occupied state at  $\Gamma$  is negligible, while the self-energy corrections for the LUMO states at  $K$  and  $M$  are both equal to  $0.6 \pm 0.1$  eV. As a result, not only is the gap opened up in the quasiparticle approach but, in addition, the ordering of the lowest conduction bands is modified. In particular, the bottom of the conduction band is displaced from  $K$  to  $\Gamma$  by the quasiparticle treatment. Therefore, within the  $GW$  approximation, the gap is indirect between  $K$  and  $\Gamma$ . We note that, because the LUMO state at  $\Gamma$  displays a nearly-free-electron-like character, it is not surprising that the LDA exchange-correlation potential and the self-energy operator yield the same expectation value for this state [see Eq. (4)].

We performed the same self-energy calculation for BN( $d=7.5$ ). The self-energy corrections to the LDA eigenvalues are similar to those obtained for BN( $d=5.5$ )

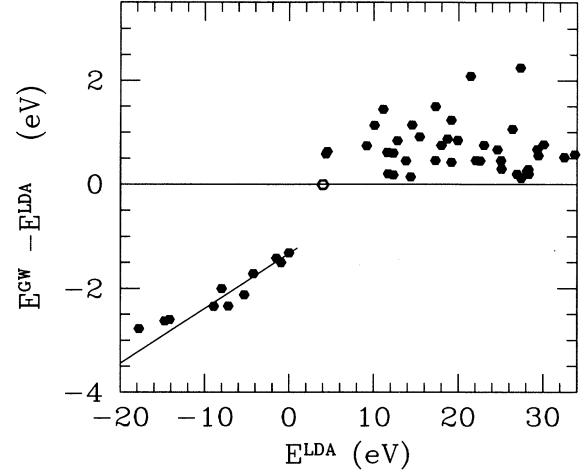


FIG. 7. The self-energy correction  $E_{nk}^{\text{qp}} - E_{nk}^{\text{LDA}}$  versus the LDA eigenvalues  $E_{nk}^{\text{LDA}}$  is represented for BN( $d=5.5$ ). The energies are in eV. The hollow hexagon represents the self-energy correction for the LUMO state at  $\Gamma$ .

within the accuracy of the method. This is exemplified in Table III for selected  $\mathbf{k}$  points. The stability of the quasiparticle corrections for  $d \geq 5.5$  Å allows us to obtain the quasiparticle band structure of the isolated boron nitride sheet. For this structure, we find the quasiparticle gap to be 6 eV and the conduction band minimum  $\Gamma$ . The gap value is intermediate between the gap for bulk hexagonal and cubic BN (respectively 5.4 and 6.3 eV within the  $GW$  approximation). We note that layer-layer interaction increases the dispersion of the electronic bands and tends to reduce the gap. This effect can be used to understand the smaller gap of bulk hexagonal BN as compared to the isolated sheet.<sup>27</sup>

TABLE III. Selected energy levels at  $\Gamma$ ,  $K$ , and  $M$  for BN( $d=5.5$ ), BN( $d=7.5$ ), and BN( $d=13.5$ ) within the LDA and  $GW$  approximation. The energies are in eV. The top of the valence band is taken to be the zero of energies for both LDA and  $GW$  results.

| $d$           | $d=5.5$ |        | $d=7.5$ |        | $d=13.5$ |        |
|---------------|---------|--------|---------|--------|----------|--------|
|               | LDA     | $GW$   | LDA     | $GW$   | LDA      | $GW$   |
| $\Gamma_{1v}$ | -17.81  | -19.74 | -17.81  | -19.75 | -17.98   | -19.92 |
| $\Gamma_{3v}$ | -5.31   | -6.21  | -5.32   | -6.23  | -5.40    | -6.31  |
| $\Gamma_{5v}$ | -1.43   | -1.64  | -1.50   | -1.61  | -1.57    | -1.68  |
| $\Gamma_{1c}$ | 3.97    | 5.52   | 4.19    | 5.58   | 4.61     | 6.00   |
| $K_{3v}$      | -14.16  | -15.82 | -14.16  | -15.84 | -14.37   | -16.05 |
| $K_{1v}$      | -7.98   | -8.84  | -7.99   | -8.86  | -8.21    | -9.08  |
| $K_{2v}$      | -7.18   | -8.37  | -7.19   | -8.40  | -7.35    | -8.56  |
| $K_{3v}$      | 0.00    | 0.00   | 0.0     | 0.0    | 0.00     | 0.00   |
| $K_{3c}$      | 4.41    | 6.45   | 4.36    | 6.46   | 4.27     | 6.37   |
| $K_{1c}$      | 12.32   | 14.44  | 12.10   | 14.16  | 11.93    | 13.99  |
| $M_{1v}$      | -14.73  | -16.42 | -14.73  | -16.05 | -14.94   | -16.26 |
| $M_{3v}$      | -8.92   | -10.15 | -8.91   | -9.92  | -9.10    | -10.11 |
| $M_{1v}$      | -4.22   | -4.72  | -4.24   | -4.73  | -4.44    | -4.93  |
| $M_{3v}$      | -0.95   | -1.15  | -0.97   | -1.08  | -0.96    | -1.07  |
| $M_{1c}$      | 4.57    | 6.65   | 4.49    | 6.39   | 4.43     | 6.33   |
| $M_{3c}$      | 9.19    | 11.42  | 9.24    | 12.26  | 9.25     | 12.27  |

We note that the present results show some discrepancies with a recent self-energy calculation<sup>3</sup> for an isolated BN sheet. The work in Ref. 3 was based on the Møller-Plesset perturbation theory and STO-3G Gaussian orbitals were used. The most important difference between the two sets of results is that the state predicted in the present work to be the bottom of the conduction band within the *GW* approximation (the LUMO state at  $\Gamma$ ) was reported to be 12.3 eV above the lowest occupied state at  $K$  in Ref. 3. This state is shown here to have a very large extension in the vacuum region. Such an extended state is easily described using a plane-wave basis. However, a localized basis such as STO-3G or a Slater-Koster-type ( $3s, 3p_x, 3p_y, 3p_z$ ) basis<sup>28</sup> would have difficulty in reproducing the extension of such a wave function away from the atoms. A previous tight-binding (TB) calculation<sup>1</sup> performed on bulk hexagonal BN shows that the LUMO state at  $\Gamma$  is (within the TB calculation) located 10 eV above its “LDA-plane-wave basis” analog (we aligned the bottom of the conduction band at  $K$  in both calculations). This is consistent with the results of Ref. 3 where the use of a limited localized basis underbinds the extended states.

#### IV. CONCLUSION

We have calculated the quasiparticle band structure of the most common allotropic form of bulk BN which is hexagonal. The band gap is indirect and calculated to be 5.4 eV (that is 0.9 eV smaller than in cubic BN). The isolated BN sheet has also been studied. The band gap

of the sheet is calculated to be 6.0 eV. The bottom of the conduction band is a state with charge density which has a very large extent into the vacuum region. This feature makes its study difficult for theoretical methods based on the use of localized bases. The present results have been used to calculate the quasiparticle band structure of BN nanotubes.<sup>2</sup> In particular, the LUMO state for these tubes is found to be a nearly-free-electron state with charge density localized along the axis of the tubes. This free-electron tubular state is derived from the LUMO state of the isolated BN sheet when the planar structure is rolled into a tubular shape. The BN tubes have been predicted theoretically to be metastable (as are their graphitic analogs), and a recent experimental study<sup>23</sup> reports the observation of  $B_xC_yN_z$  nanotubes. Therefore it would be most relevant and interesting to apply the present self-energy method to  $BC_3$  and  $BC_2N$  hexagonal structures.

#### ACKNOWLEDGMENTS

This work was supported by National Science Foundation Grant No. DMR-9120269 and by the Director, Office of Energy Research, Office of Basic Energy Sciences, Materials Sciences Division of the U.S. Department of Energy under Contract No. DE-AC03-76SF00098. Supercomputer time was provided by the NSF Pittsburgh Supercomputer Center. We thank Dr. Yoshimori Miyamoto for useful discussions. A.R. is supported by the Fullbright Commission.

- 
- <sup>1</sup> A. Rubio, J. Corkill, and M. L. Cohen, *Phys. Rev. B* **49**, 5081 (1994).
- <sup>2</sup> X. Blase, A. Rubio, S. G. Louie, and M. L. Cohen, *Euro. Phys. Lett.* **28**, 335 (1994).
- <sup>3</sup> K. Kobayashi, T. Sano, and Y. J. I'Haya, *Chem. Phys. Lett.* **219**, 53 (1994).
- <sup>4</sup> C. A. Brookes, R. M. Hooper, and W. A. Lambert, *Philos. Mag. A* **47**, L9 (1983).
- <sup>5</sup> BN can be found in the zinc-blende, wurtzite, or hexagonal structure. The hexagonal (graphitelike) structure is the most common form of BN. Cubic BN has been studied within the same quasiparticle approach. See M. P. Surh, S. G. Louie, and M. L. Cohen, *Phys. Rev. B* **43**, 9126 (1991).
- <sup>6</sup> M. S. Hybertsen and S. G. Louie, *Phys. Rev. Lett.* **55**, 1418 (1985); *Phys. Rev. B* **34**, 5390 (1986). See also R. W. Godby, M. Schlüter, and L. J. Sham, *Phys. Rev. Lett.* **56**, 2415 (1986); *Phys. Rev. B* **37**, 10 159 (1988).
- <sup>7</sup> L. Hedin, *Phys. Rev.* **139**, A796 (1965); L. Hedin and S. Lunqvist, in *Solid State Physics: Advances in Research and Applications*, edited by F. Seitz, D. Turnbull, and H. Ehrenreich (Academic, New York, 1969), Vol. 23, p. 1.
- <sup>8</sup> X. Zhu and S. G. Louie, *Phys. Rev. B* **43**, 14 142 (1991).
- <sup>9</sup> O. Zakharov, A. Rubio, X. Blase, M. L. Cohen, and S. G. Louie, *Phys. Rev. B* **50**, 10 780 (1994).
- <sup>10</sup> M. S. Hybertsen and S. G. Louie, *Phys. Rev. B* **38**, 4033 (1988).
- <sup>11</sup> X. Blase, X. Zhu, and S. G. Louie, *Phys. Rev. B* **49**, 4973 (1994), and references therein.
- <sup>12</sup> S. B. Zhang, D. Tománek, S. G. Louie, M. L. Cohen, and M. S. Hybertsen, *Solid State Commun.* **66**, 585 (1988).
- <sup>13</sup> M. S. Hybertsen and M. Schlüter, *Phys. Rev. B* **36**, 9683 (1987); S. B. Zhang, M. S. Hybertsen, M. L. Cohen, S. G. Louie, and D. Tománek, *Phys. Rev. Lett.* **63**, 1495 (1989).
- <sup>14</sup> E. Shirley and S. G. Louie, *Phys. Rev. Lett.* **71**, 133 (1993).
- <sup>15</sup> N. Troullier and J. L. Martins, *Solid State Commun.* **74**, 613 (1990); *Phys. Rev. B* **43**, 1993 (1991).
- <sup>16</sup> D. M. Ceperley and B. J. Alder, *Phys. Rev. Lett.* **45**, 566 (1980).
- <sup>17</sup> H. J. Monkhorst and J. D. Pack, *Phys. Rev. B* **13**, 5188 (1976).
- <sup>18</sup> M. S. Hybertsen and S. G. Louie, *Phys. Rev. B* **35**, 5585 (1987).
- <sup>19</sup> S. L. Adler, *Phys. Rev.* **126**, 413 (1962).
- <sup>20</sup> N. Wiser, *Phys. Rev.* **129**, 62 (1963).
- <sup>21</sup> R. M. Wentzcovitch, K. J. Chang, and M. L. Cohen, *Phys. Rev. B* **34**, 1071 (1986). In this study, the LDA minimum band gap was found to be 4.2 eV.
- <sup>22</sup> N. E. Christensen and I. Gorczyca, *Phys. Rev. B* **50**, 4397 (1994). In this study, the LDA band gap was found to be 5.4 eV for wurtzite BN and 4.4 eV for the zinc-blende structure.
- <sup>23</sup> Synthesis of  $B_xC_yN_z$  nanotubes has been recently reported. In these structures, electron energy loss spectroscopy measurements show that the nitrogen  $K$  edge differs significantly from the usual  $sp^2$  hybridization shape. See K. Cherey *et al.* (unpublished).

<sup>24</sup> The LUMO state at  $\Gamma$  is located 1.14 eV below the vacuum level.

<sup>25</sup> An equivalent state has been shown to exist in the graphene sheet using the same supercell method [Y. Miyamoto (private communication)].

<sup>26</sup> D. Tománek and S. G. Louie, Phys. Rev. B **37**, 8327 (1988).

<sup>27</sup> In the case of bulk hexagonal BC<sub>3</sub>, the gap closes only because of the band structure dispersion along the *c* axis. See Y. Miyamoto, A. Rubio, M. L. Cohen, and S. G. Louie,

Phys. Rev. B **50**, 18 360 (1994).

<sup>28</sup> We note that the STO-*n*G basis consists of expansions of Slater-type atomic orbitals in terms of *n* Gaussian functions. Therefore both bases are equivalent and, in particular, have the same spatial extent. For a review, see W. J. Wehre, L. Radom, P. v. R. Schleyer, and J. A. Pople, *Ab Initio Molecular Orbital Theory* (John Wiley & Sons, Inc., New York, 1986).